Surface & Coatings Technology 206 (2012) 4692–4703

Contents lists available at SciVerse ScienceDirect

Surface & Coatings Technology

journal homepage: www.elsevier.com/locate/surfcoat

Assessment of duplex coating combining plasma electrolytic oxidation and polymer layer on AZ31 magnesium alloy

R. Arrabal [a,*], J.M. Mota [b], A. Criado [a], A. Pardo [a], M. Mohedano [a], E. Matykina [a]

[a] Departamento de Ciencia de Materiales, Facultad de Ciencias Químicas, Universidad Complutense, 28040, Madrid, Spain
[b] Desarrollo y Control Tecnológico, S.L. Pol. Ind. Casarrubios Nave B-3, 28806 Alcalá de Henares, Spain

ARTICLE INFO

Article history:
Received 16 December 2011
Accepted in revised form 22 May 2012
Available online 1 June 2012

Keywords:
Magnesium
Plasma electrolytic oxidation
Corrosion
Polymer coating
Impact
ac/dc/ac

ABSTRACT

Mechanical and corrosion tests were performed on a polymer-coated AZ31 magnesium alloy pre-treated by plasma electrolytic oxidation (PEO). Results were compared with a fluorotitanate–zirconate conversion coating pre-treatment. Mechanical performance was assessed by standardized adhesion (ISO 2409:2007), impact (ISO 6272-1:2004) and impact + adhesion (ISO 6272/ASTMD2794) pass/fail tests. Corrosion behavior was monitored using electrochemical impedance spectroscopy (EIS), ac/dc/ac measurements and continuous exposure to salt fog per ASTM B117 and cyclic exposure per VDA 621-415 (VDA). The PEO + polymer coating revealed lower impact resistance but better corrosion resistance than the Ti/Zr + polymer coating. The ac/dc/ac procedure demonstrated to be faster than EIS measurements for evaluation of the corrosion performance of studied coatings.

1. Introduction

Magnesium alloys are rapidly becoming the material of choice in weight restricted applications, such as aerospace and automotive components, due to their low density and high strength-to-weight ratio [1]. However, their poor corrosion resistance demands surface treatments, which commonly include conversion coatings, anodizing, polymer coatings, gas phase deposition, thermal/cold spraying, electro/electroless plating and, more recently, plasma electrolytic oxidation (PEO) [2–9].

In the particular case of polymer coatings, surface pre-treatment is essential in order to ensure adequate corrosion protection and adhesion bonding with the substrate. For magnesium alloys, surface pre-treatments based on chromate conversion coatings have been widely used. These treatments form complex chromate-based films on the surface with self-healing properties due to the presence of hexavalent chromium [10]. However, according to the 2000/53/EC directive, vehicles put on the market after 1 July 2003 must not contain hexavalent chromium. This has led to the development of alternative conversion coatings such as those based on manganate/molybdate and fluorozirconate–fluorotitanate solutions [10]. In the latter case, the metal substrate is exposed to an aqueous acidic solution containing titanium/zirconium hexafluorides and a continuous three-dimensional polymeric metal matrix is believed to form on the surface [11]. These treatments offer good paint adhesion [12] and adequate performance in mild corrosive environments [13]. However, they are not suitable for use in severe corrosive environments and more efficient pre-treatments are needed. Previous studies have demonstrated that, among the existing alternatives, superior corrosion resistance can be achieved using PEO as a pre-treatment for polymer coatings [14–20].

The PEO process, also known as microarc oxidation [7], produces relatively thick ceramic-like coatings under high voltages in environmentally friendly electrolytes, usually comprising silicate, phosphate, aluminate or fluoride salts in low concentrations [21]. The average growth rate is between 1 and 10 μm/min and the coatings typically consist of a thin barrier layer adjacent to the substrate and one or more outer layers [8], whose thicknesses and characteristics depend on the applied electric signal and the substrate/electrolyte combination [22]. The main advantages of PEO coatings include improved corrosion and wear resistance, high dielectric strength, heat resistance and suitable surface morphology for topcoat paints and other metals/ceramics to create duplex coatings [23]. However, in corrosion sensitive applications, PEO coatings are prone to failure due to their permeability to

Table 1
Chemical composition of AZ31 magnesium alloy.

Material	Chemical composition (wt.%)									
	Al	Zn	Mn	Si	Cu	Fe	Ni	Ca	Zr	Others
AZ31	3.1	0.73	0.25	0.02	<0.001	0.005	<0.001	<0.01	<0.001	<0.30

* Corresponding author. Tel.: +34 91 3945227; fax: +34 91 3944357.
E-mail address: raularrabal@quim.ucm.es (R. Arrabal).

0257-8972/$ – see front matter © 2012 Elsevier B.V. All rights reserved.
doi:10.1016/j.surfcoat.2012.05.091

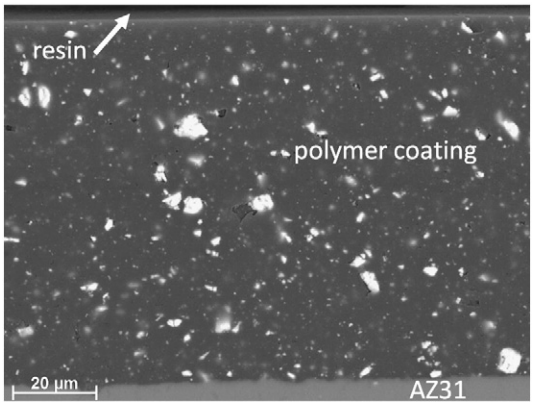

Fig. 1. BSE micrograph of the cross-section of AZ31 magnesium alloy with the Ti/Zr + polymer coating.

the environment [24]. Enhanced corrosion resistance of PEO coatings is achieved either by adjusting the electrolyte composition and process parameters or by sealing active points such as coating pores and cracks. Existing sealing techniques include immersion in phosphate, silicate or borate-containing solutions and other approaches such as sol–gel, polymers, etc. [14–21,25–31].

Accelerated atmospheric corrosion tests and electrochemical impedance spectroscopy (EIS) have been widely used for quality control of polymer-coated metal surfaces. However, these laboratory corrosion tests take a long time and new methods are required for purposes of rapid comparison of corrosion resistance of different coating systems. Hollaender et al. [32] developed a procedure consisting of a combination of ac and dc measurements, namely ac/dc/ac procedure, which has been successfully employed to evaluate the corrosion resistance of coated steel, aluminum and, more recently, magnesium [33,34] in relatively short times in comparison with EIS measurements. In this procedure, an ac scan is run to establish the initial condition of the coating, then

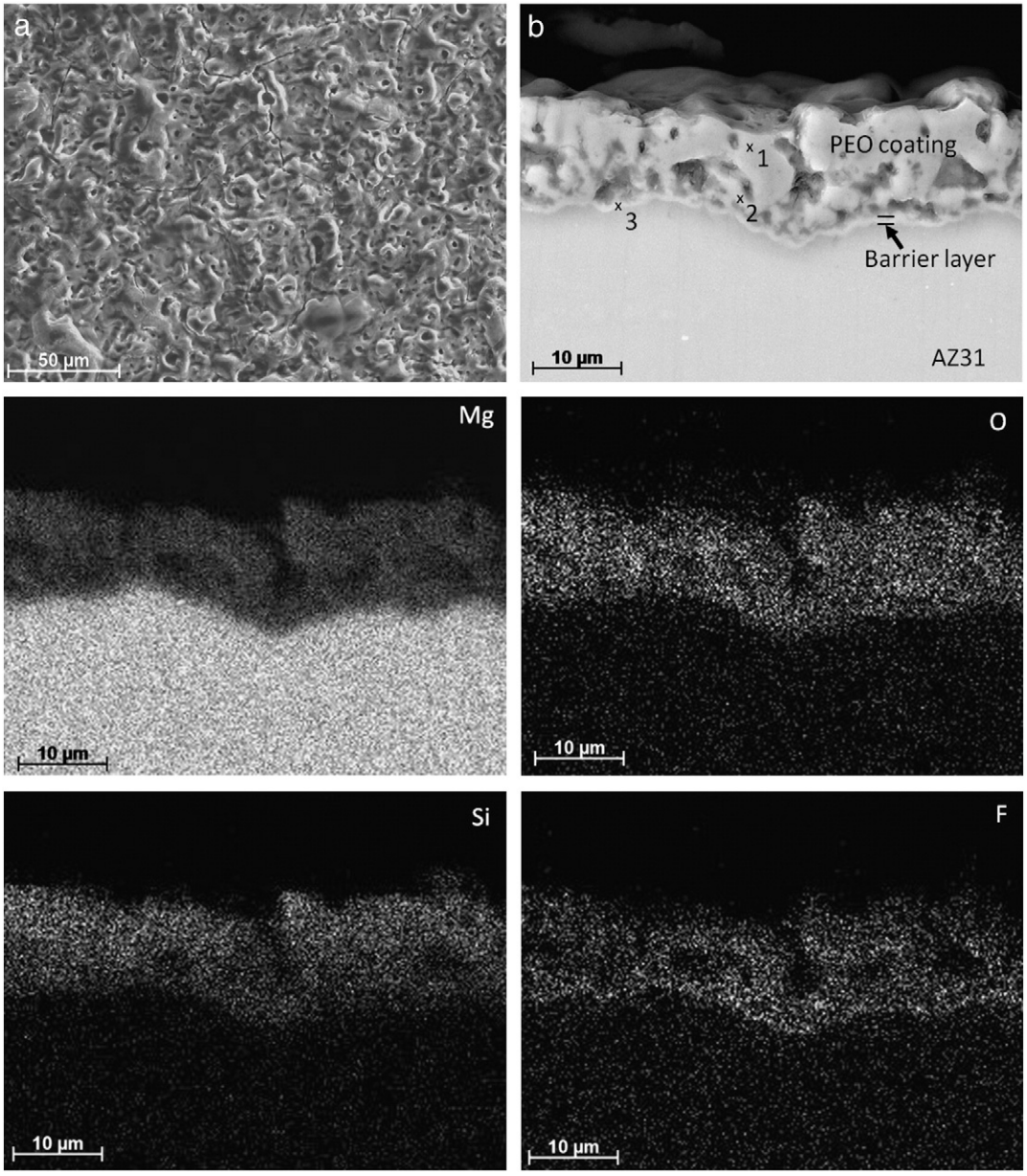

Fig. 2. (a) SEM plan view and (b) BSE cross-section and X-ray maps of PEO-treated AZ31 magnesium alloy.

Table 2
EDX results of points 1, 2 and 3 in Fig. 2.

	Elements (at.%)				
	Mg	Al	F	Si	O
1	35.7	1.1	17.5	12.9	32.8
2	40.9	1.9	30.4	5.2	21.7
3	69.8	2.3	14.2	1.9	11.8

the sample is cathodically polarized to generate an alkaline environment and stimulate coating deterioration and, finally, another ac scan is run to assess the new coating condition [35]. The process may be repeated to apply additional stress to the sample.

In the present study, pass/fail mechanical tests and accelerated corrosion tests under continuous and cyclic salt fog were carried out on polymer-coated AZ31 magnesium alloy. Two pre-treatments were compared, namely an oxide film formed by PEO and a commercial fluorotitanate–zirconate conversion coating. Additionally, the electrochemical behavior of the coatings was assessed using EIS measurements and the ac/dc/ac accelerated test, which, to the best of the authors' knowledge, has not yet been used for duplex PEO + polymer coatings on magnesium alloys.

2. Experimental

2.1. Material

AZ31 magnesium alloy sheet, supplied by Magnesium Elektron Ltd. (U.K.), with a chemical composition shown in Table 1 was used in this study.

2.2. Surface pre-treatments

2.2.1. PEO treatment

Prior to PEO treatment, samples were ground to P1200 grit silicon carbide using water as a lubricant, degreased in ethanol, rinsed in deionized water and dried in warm air. A working area of ~45 cm^2 was defined in AZ31 panels (130 mm × 80 mm × 2 mm) by application of Lacquer 45 resin (MacDermid plc). Electrical connection was provided through a copper wire. PEO treatment was carried out for 600 s using an EAC-S2000 power supply (ET systems electronic). The electrical parameters were fixed as follows: frequency 50 Hz, positive voltage = 425 V, negative voltage = 50 V, duty cycle = 50% and current limit = 260 mA/cm^2 (rms). The electrolyte, comprising 10 g/L $Na_2SiO_3 \cdot 5H_2O$ and 5 g/L NaF, prepared from deionized water and high-purity chemicals, was continuously stirred during the treatment. The coatings were formed in a 1 L double-walled glass cell through which cooled water was pumped to maintain the electrolyte temperature close to 22 °C. A sheet of type 316 stainless steel, with the dimensions of 7.5 × 15 cm, was used as a cathode. After coating, specimens were rinsed with deionized water and dried in warm air.

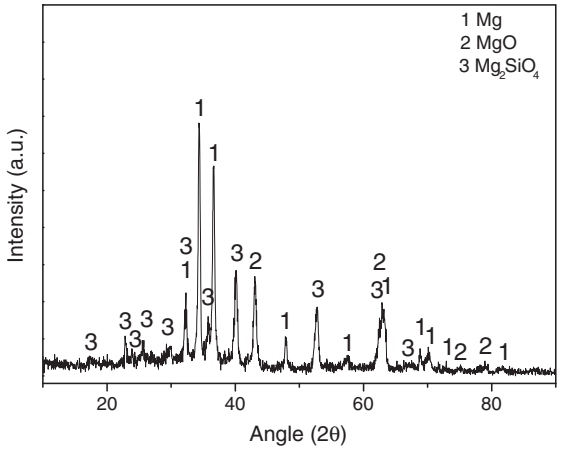

Fig. 3. XRD pattern of PEO coating formed on AZ31 magnesium alloy.

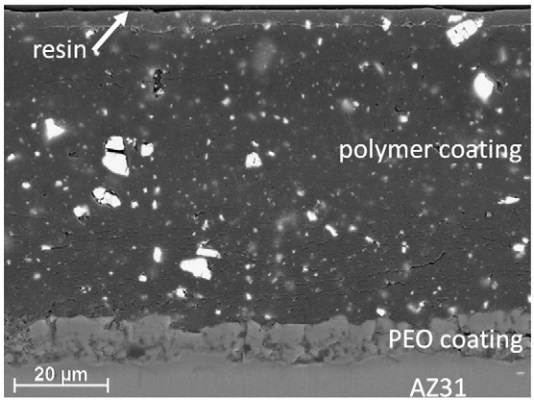

Fig. 4. BSE micrograph of the cross-section of AZ31 magnesium alloy with the PEO + polymer coating.

2.2.2. Fluorotitanate–zirconate treatment

The following general procedure was used to produce the Ti/Zr conversion layer:

1. Alkaline etch in 20 g/L KOH solution, 50 °C, 5 min.
2. Rinse with tap water and deionized water.
3. Neutralization in an acid bath (10 g/L HNO_3/HF), 25 °C, 10 s.
4. Conversion coating in fluorotitanate/zirconate acid based solution (4% Gardobond X4707), pH 3, 25 °C, 30 s.
5. Rinse with tap and deionized water.
6. Dry in hot air stream.

2.3. Electrostatic spray paint

A proprietary polyester-based polymer with high gloss and good color retention for outdoor applications was selected for this study. The polymer consisted of the following:

- Polyester resin (50 wt.%). This resin provides a good combination of gloss and mechanical properties.
- Triglycidyl isocyanurate hardener, which is normally used in exterior quality polyester powder systems.
- Polypropylene wax (≤1 wt.%) additive, used to increase the paint hardness and scratch resistance.

Table 3
Results of the mechanical tests of polymer and PEO + polymer coatings.

		Ti/Zr + polymer	PEO + polymer
Paint adhesion		0	0
	Height (cm)		
Impact	25	0	0
	30	0	0
	50	0	Failed
	100	0	Failed
Impact + adhesion	25	0	0
	30	0	Failed
	50	0	Failed
	100	0	Failed

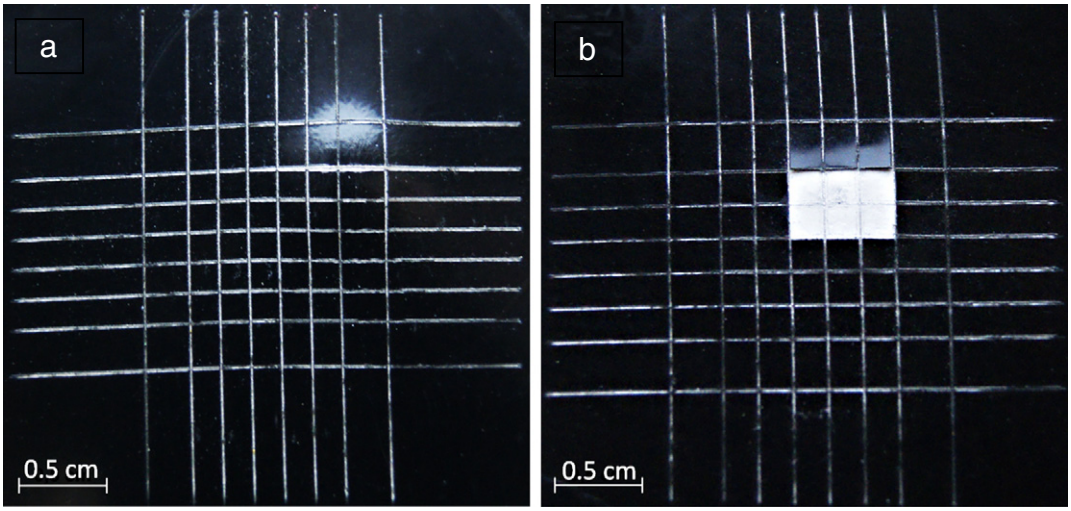

Fig. 5. Surface appearance of (a) Ti/Zr + polymer and (b) PEO + polymer coatings after impact + adhesion tests.

- Inorganic pigments capable of withstanding the temperatures used in the polymerization process.
- Fillers (barium carbonate and barium sulfate). Barium salts reduce the excessive gloss provided by the resin and improve the mechanical and esthetic properties of the finished product.

The polymer was applied using an electrostatic spray system (Ransburg GEMA AG., Electrostatic Gun PG 1-A) and cured at 200 °C for 20 min. No special pre-treatment was required for painting the PEO coated specimens. From this point on, the term "Ti/Zr + polymer" refers to the specimens pre-treated with the Ti/Zr conversion coating followed by polymer layer. PEO treated specimens followed by polymer layer are referred to as "PEO + polymer".

2.4. Mechanical tests

AZ31 panels (130 mm × 80 mm × 2 mm) with Ti/Zr + polymer and PEO + polymer coatings were tested for cross cut adhesion per ISO 2409:2007 [36]. The coatings were cut through in six lines (2 mm spacing) using a cutting blade. This cutting guide was then rotated 90° and another six lines were cut through the coatings, leaving behind a grid with 25 squares. Standard pressure-sensitive tape was applied to the grid and removed evenly within 5 min of applying the tape.

The evaluation of impact resistance of the coatings applied on the AZ31 panels was carried out in accordance with ISO 6272-1:2002 standard [37]. In this test, a spherical indenter of diameter 20 mm impacts the coated sample on the back side. The drop height is adjusted to 25–100 cm to obtain a given impact energy. The adherence of the coating on the top side is checked using adhesive tape.

2.5. Corrosion tests

2.5.1. EIS measurements

An AUTOLAB PGSTAT 30 computer-controlled potentiostat (Eco Chemie) equipped with a frequency response analyzer and connected to a three-electrode cell was used for the electrochemical measurements. The working electrode was the test material with an immersed area of ~13 cm^2. Graphite and silver/silver chloride (Ag/AgCl) electrodes were used as the counter and reference electrodes, respectively. Solution concentration inside the reference electrode compartment was

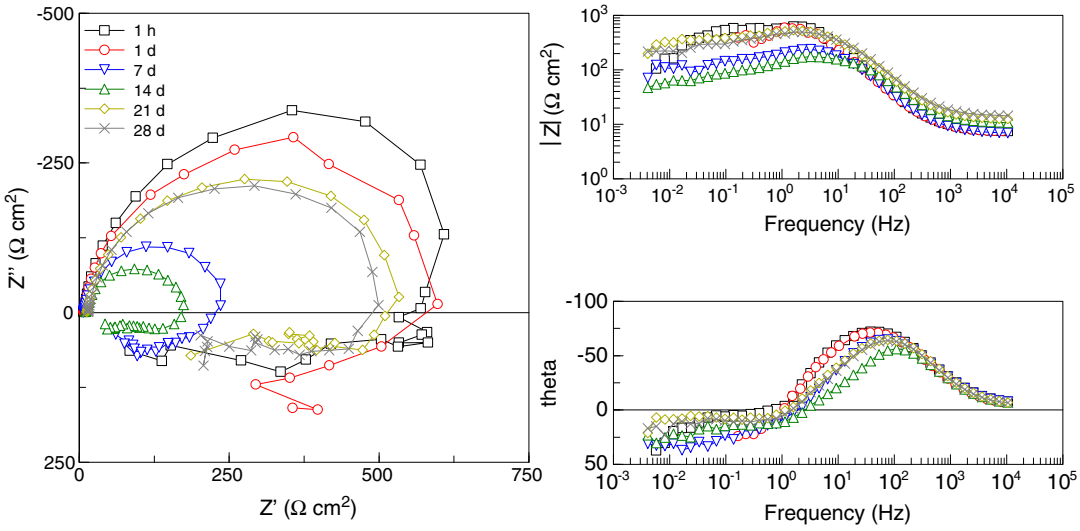

Fig. 6. Nyquist and Bode plots of AZ31 alloy.

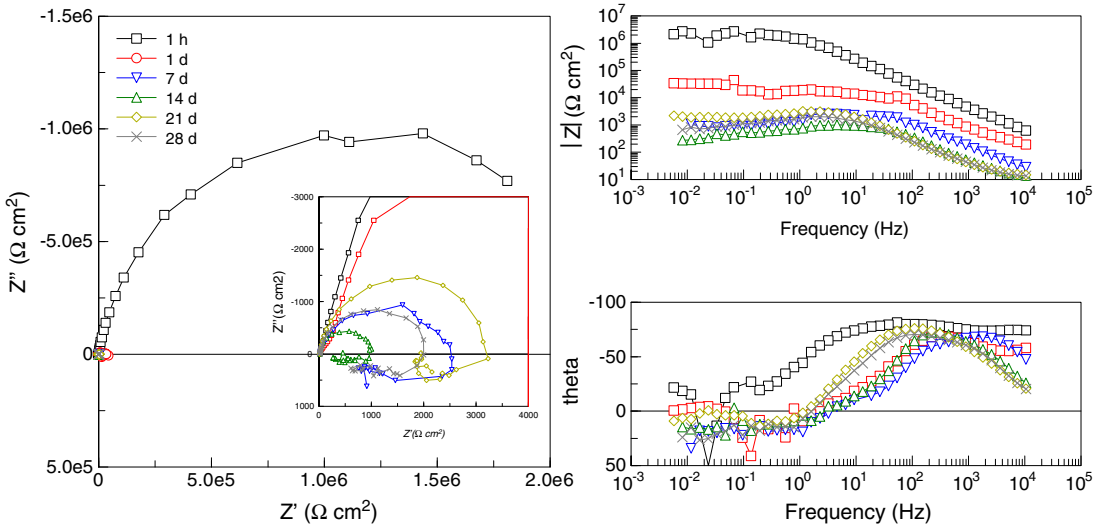

Fig. 7. Nyquist and Bode plots of PEO-coated AZ31 alloy.

3 M KCl, providing a potential of 0.197 V with respect to the standard hydrogen electrode. The test solution was naturally-aerated 5 wt.% NaCl solution at room temperature (22 °C) and pH 6.5.

EIS measurements were conducted at various times up to 77 days of immersion. The frequency range was from 10 kHz to 2 mHz and the amplitude of the sinusoidal potential signal was 10 mV with respect to the open circuit potential (OCP). Measurements were performed three times to ensure reproducibility of the results. The impedance spectra were analyzed using ZView™ (Scribner Associates Inc.) electrochemical analysis software.

2.5.2. ac/dc/ac procedure

The ac/dc/ac method was employed on polymer-coated specimens and comprised three steps. First, an ac test is applied to the sample under the same conditions as described in Section 2.5.1. Then, the sample is polarized under a constant cathodic voltage (−4 V vs. OCP) for 30 min (dc) and, after that, the cathodic potential is removed to trigger a relaxation process that takes about 3 h. Finally, an ac test is conducted again on the relaxed sample. All cycles were fully automated in AUTOLAB PGSTAT30 potentiostat. This sequence was repeated up to 70 cycles, with a duration of 4 h per cycle, till corrosion damage was visually observed.

2.5.3. Atmospheric corrosion tests

Uncoated and coated AZ31 panels (80 mm × 25 mm × 2 mm) were exposed to continuous salt fog per ASTM B117 [38] and cyclic exposure per VDA 621-415 (VDA) [39] standards in an automatic CCI climatic chamber. The exposed surface area was ~13 cm^2. The cycle VDA test consisted of the following:

a) 1 day salt fog test according to ASTM B117.
b) 4 days cyclic humidity. Each cycle comprised 3 h at 40 °C and 98% relative humidity followed by 16 h at 23 °C and 50% relative humidity.
c) 2 days ambient climate according to DIN 50014 [40].

In order to determine the development of corrosion in an abraded area in the applied polymer-based coatings, a scribed line was made with a scalpel blade so as to expose the underlying metal before testing. Rating of the coatings was assessed in accordance with ASTM D1654 standard [41].

2.6. Specimen examination

Specimens were examined by scanning electron microscopy using a JEOL JSM-6400 instrument equipped with Oxford Link energy-dispersive X-ray (EDX) microanalysis hardware. Cross-sections were ground through successive grades of SiC paper, followed by diamond finishing to 1 μm. At 20 randomly selected places, the thicknesses of the coatings were measured using an eddy-current meter (Isoscope

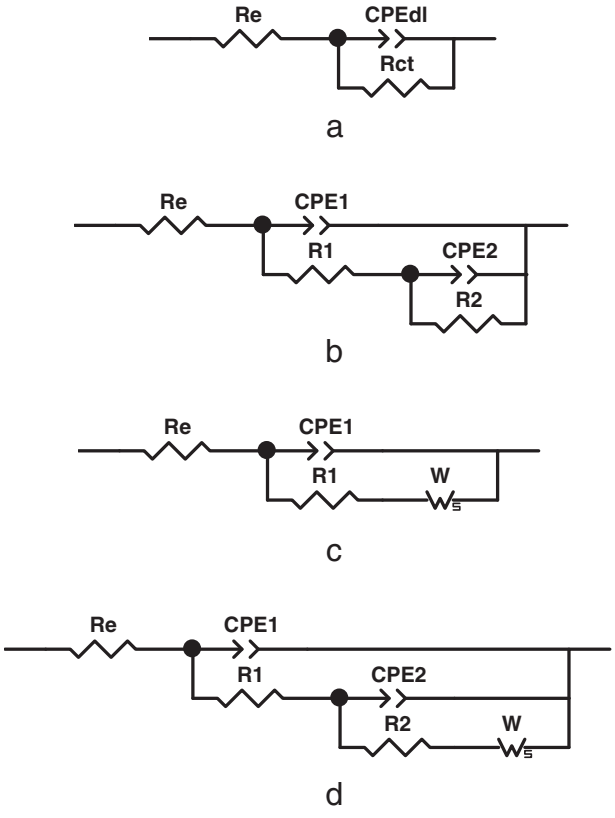

Fig. 8. Equivalent circuits proposed for (a) AZ31 alloy, (b) PEO-coated AZ31 alloy and polymer-coated specimens after failure and (c, d) polymer-coated specimens before failure.

Table 4
Data of the equivalent circuits of untreated and PEO-treated AZ31 alloy.

	1 h	1 days	7 days	14 days	21 days	28 days
AZ31						
OCP ($V_{Ag/AgCl}$)	−1.539	−1.546	−1.538	−1.520	−1.517	−1.521
CPE_{dl}-*T* ($S\ s^P/cm^2$)	6.54×10^{-5}	7.68×10^{-5}	8.81×10^{-5}	6.38×10^{-5}	5.01×10^{-5}	4.40×10^{-5}
CPE_{dl}-*P*	0.94	0.93	0.91	0.89	0.89	0.90
R_{ct} ($\Omega\ cm^2$)	628	612	248	166	549	504
AZ31 PEO						
OCP ($V_{Ag/AgCl}$)	−1.438	−1.530	−1.513	−1.512	−1.510	−1.520
CPE_1-*T* ($S\ s^P/cm^2$)	2.61×10^{-8}	9.95×10^{-8}	5.41×10^{-7}	2.33×10^{-6}	5.60×10^{-6}	9.72×10^{-6}
CPE_1-*P*	0.99	0.95	0.88	0.99	0.94	0.90
R_1 ($\Omega\ cm^2$)	3786	340	9	75	92	373
CPE_2-*T* ($S\ s^P/cm^2$)	7.50×10^{-8}	5.11×10^{-7}	2.21×10^{-6}	2.07×10^{-6}	2.20×10^{-6}	1.60×10^{-6}
CPE_2-*P*	0.84	0.86	0.88	0.97	0.95	0.98
R_2 ($\Omega\ cm^2$)	2.36×10^6	15,582	2179	896	3252	1742

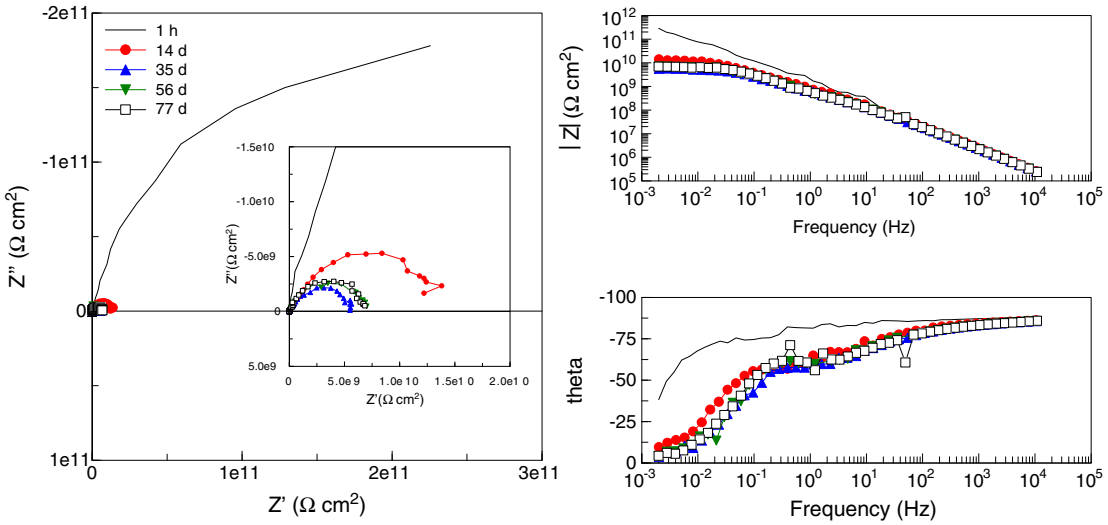

Fig. 9. Nyquist and Bode plots of Ti/Zr + polymer specimen.

FMP10, Fischer, Germany). Surface roughness was measured in five different locations using Surtronic 25 tester (Taylor Hobson Precision, UK). The evaluation length for each measurement was 25 mm. Phase composition was investigated by X-ray diffraction (XRD), using a Philips X'Pert-MPD (PW 3040) instrument with a step size of 0.005° and a scan range from 10 to 80° (in 2θ).

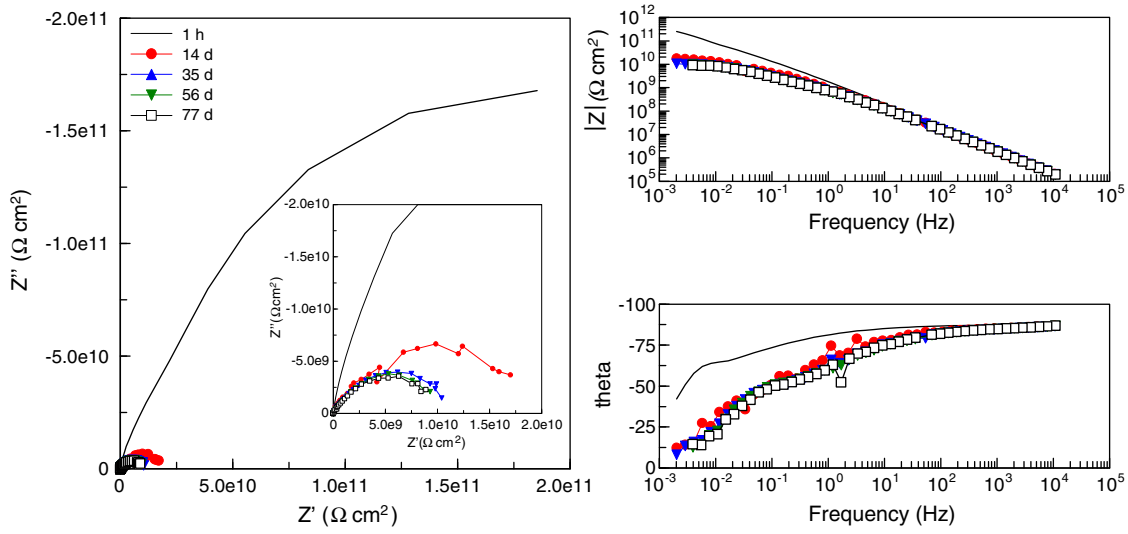

Fig. 10. Nyquist and Bode plots of PEO + polymer specimen.

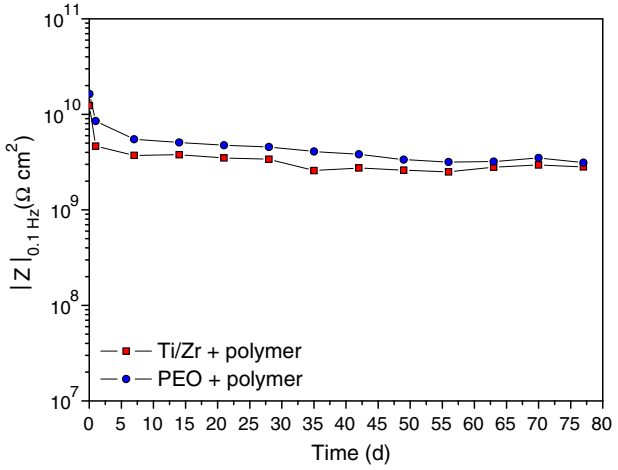

Fig. 11. Low-frequency impedance modulus of Ti/Zr + polymer and PEO + polymer specimens as a function of immersion time in 5 wt.% NaCl.

3. Results and discussion

3.1. Specimens characterization

Fig. 1 shows the backscattered scanning electron (BSE) micrograph of the cross-section of the Ti/Zr + polymer coating applied on the AZ31 magnesium substrate. The coating was uniform in thickness (81 ± 2 μm) and R_a and R_z roughness values were 0.077 ± 0.003 μm and 0.65 ± 0.04 μm, respectively. Barium sulfate and barium carbonate particles with good bonding to the polyester matrix were clearly visible. The Ti/Zr conversion layer, possibly of a few nanometers thickness [42], was not observed at the used magnification.

Fig. 2a and b shows the plan view and cross-section BSE micrographs of the PEO coating formed on the AZ31 magnesium alloy. The typical morphology of PEO coatings with numerous pores, which occupied ~4% of the surface and revealed an average size in the range of 1–6 μm, was observed in Fig. 2a. PEO coating thickness was estimated to be 15 ± 2 μm and roughness values were higher than those of the polymer coating ($R_a = 1.07 \pm 0.06$ μm, $R_z = 7.5 \pm 0.5$ μm). Examination of the cross-section revealed a scalloped substrate/coating interface due to local thickening of the coating following dielectric breakdown events (Fig. 2b). Fig. 2b and X-ray maps disclosed three layers: a 650 nm-thick barrier layer, possibly consisting of MgO enriched with F; an F-rich inner layer with relatively small pores; and an outer Si-rich layer with larger pores (Table 2). The latter constituted less than 50% of the coating thickness and protruded slightly above the original untreated surface. XRD measurements following PEO treatment for 600 s revealed MgO and Mg_2SiO_4 as the main components of the PEO coating (Fig. 3).

The BSE micrograph of the cross-section of the PEO + polymer coating is presented in Fig. 4. Surface roughness was very similar to that measured for the Ti/Zr + polymer coating ($R_a = 0.076 \pm 0.003$ μm, $R_z = 0.68 \pm 0.03$ μm), whereas the polymer coating thickness was slightly smaller (78 ± 1 μm), possibly due to the dielectric nature of the PEO coating during electrostatic spray painting.

3.2. Mechanical tests

Table 3 shows the results of mechanical tests performed on the AZ31 magnesium alloy with the Ti/Zr + polymer and PEO + polymer coatings. Both coatings passed the adhesion test (rating 0) since the edges of the cuts were completely smooth and none of the squares of the lattice were detached.

Results of impact and impact + adhesion tests revealed better performance of the Ti/Zr + polymer coating compared with the PEO + polymer coating, which failed the impact test for 50 and 100 cm drop heights and the impact + adhesion test (Fig. 5) for drop heights above 25 cm. This was not surprising considering the ceramic-like structure of the PEO coating, which is also known to cause a reduction in the fatigue performance [17] of magnesium alloys due to several factors, including structural defects in the oxide layer and a substantial lattice misfit between the oxide and the metal [43].

3.3. Corrosion tests

3.3.1. EIS results

Figs. 6 and 7 show the impedance spectra of AZ31 alloy without and with PEO treatment after immersion in 5 wt.% NaCl solution for different times up to 28 days. Nyquist plots of untreated AZ31 alloy were characterized by a capacitive loop at high and medium frequencies, followed by an inductive loop in the low frequency region (Fig. 6). The capacitive loop was attributed to the charge transfer resistance and double electric layer capacitance at the metal/solution interface,

Table 5
Data of the equivalent circuits of polymer-coated specimens.

	1 h	14 days	35 days	56 days	77 days
Ti/Zr + polymer					
OCP ($V_{Ag/AgCl}$)	−1.192	−1.238	−1.212	−1.227	−1.195
CPE_1-*T* (S s^P/cm^2)	4.31×10^{-11}	5.62×10^{-11}	5.81×10^{-11}	5.84×10^{-11}	5.89×10^{-11}
CPE_1-*P*	0.98	0.99	1.00	1.00	1.00
R_1 (Ω cm^2)	2.41×10^{8}	2.54×10^{6}	1.66×10^{6}	1.36×10^{6}	1.56×10^{6}
CPE_2-*T* (S s^P/cm^2)	--	1.39×10^{-10}	2.31×10^{-10}	1.98×10^{-10}	2.16×10^{-10}
CPE_2-*P*	–	0.72	0.69	0.69	0.68
R_2 (Ω cm^2)	–	5.26×10^{8}	4.76×10^{8}	3.99×10^{8}	3.75×10^{8}
W-*R* (Ω cm^2)	3.21×10^{11}	1.31×10^{10}	5.30×10^{9}	6.63×10^{9}	6.81×10^{9}
W-*T* (s)	100.1	8.8	3.1	2.4	2.4
W-*P*	0.59	0.48	0.53	0.62	0.61
PEO + polymer					
OCP ($V_{Ag/AgCl}$)	−1.201	−1.241	−1.186	−1.235	−1.199
CPE_1-*T* (S s^P/cm^2)	6.44×10^{-11}	7.21×10^{-11}	7.28×10^{-11}	7.37×10^{-11}	7.31×10^{-11}
CPE_1-*P*	0.97	0.99	1.00	1.00	1.00
R_1 (Ω cm^2)	3.56×10^{7}	2.32×10^{6}	1.97×10^{6}	2.27×10^{6}	2.17×10^{6}
CPE_2-*T* (S s^P/cm^2)	–	1.71×10^{-10}	1.77×10^{-10}	1.26×10^{-10}	1.17×10^{-10}
CPE_2-*P*	–	0.70	0.72	0.75	0.77
R_2 (Ω cm^2)	–	6.61×10^{9}	1.13×10^{9}	8.22×10^{8}	1.03×10^{9}
W-*R* (Ω cm^2)	2.90×10^{11}	1.24×10^{10}	1.03×10^{10}	1.01×10^{10}	9.49×10^{9}
W-*T* (s)	103.9	24.5	14.2	16.0	15.5
W-*P*	0.59	0.47	0.43	0.43	0.42

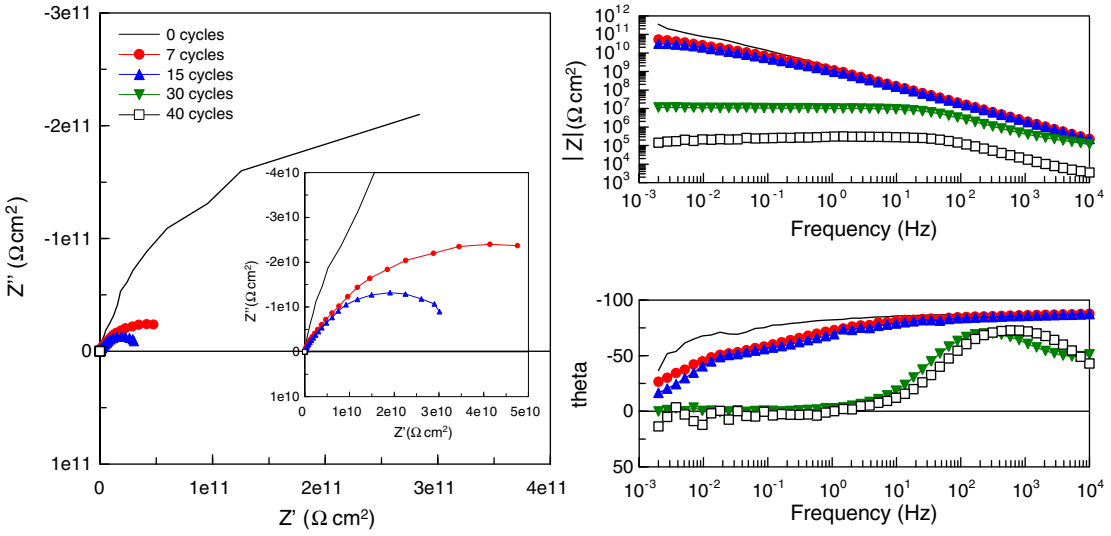

Fig. 12. Nyquist and Bode plots of Ti/Zr + polymer specimen (ac/dc/ac procedure).

whereas the inductive behavior has been associated with high concentration of Mg ions in relatively film-free areas or with an intermediate step in the corrosion process involving the presence of adsorbed surface species, such as $Mg(OH)^{+}_{ads}$, $Mg(OH)_{2\ ads}$ and Mg^{+}_{ads} [44], which is taken as an indication of pitting corrosion [45]. As shown in the Bode plot (Fig. 6), the impedance modulus at low frequencies decreased during the first 14 days of immersion, indicating continuous dissolution of the magnesium matrix. However, it increased again at 21 and 28 days, suggesting the formation of a layer of corrosion products that delayed the permeation of corrosive electrolyte to the substrate. This layer was not very protective as evidenced by the presence of the inductive loop for all the immersion times tested.

The Nyquist plot for the PEO-treated alloy revealed a partially resolved capacitive loop after 1 h of immersion (Fig. 7) and, as suggested by the high impedance values, the coating did not undergo any significant degradation. However, after 1 day of exposure, the impedance dropped substantially, indicating degradation of the PEO coating. This was evident from the emergence of an inductive loop in the Nyquist plot [45] and the presence of macroscopic corrosion pits, which were clearly visible after immersion times above 7 days.

The simplified equivalent circuits employed for curve fitting of the untreated and PEO-treated AZ31 alloys are illustrated in Fig. 8a and b, respectively. It should be noted that the electrochemical behavior at low frequencies was not analyzed since it was not reproducible, possibly due to corrosion damage. In the equivalent circuit proposed for the AZ31 alloy, R_e is the resistance of the electrolyte between reference and working electrodes, R_{ct} is the charge transfer resistance and CPE_{dl} is a constant phase element related to the double electric layer capacitance. The impedance of a constant phase element is described as:

$$Z_{CPE} = \frac{1}{T(j\omega)^{P}} \tag{1}$$

where T is the CPE constant, which nominally equals to admittance of the system at 1 rad/s; $j = \sqrt{-1}$, ω is the angular frequency (rad/s) and the value of P ranges between 0 and 1. If $P = 1$, Eq. (1) becomes the impedance of a pure capacitor; if $P = 0$, CPE acts as a pure resistor. The equivalent circuit chosen to model the PEO-treated alloy system comprises R_e, CPE_1R_1 (capacitive behavior and resistance of the outer porous part of the coating or the layer of corrosion products formed after

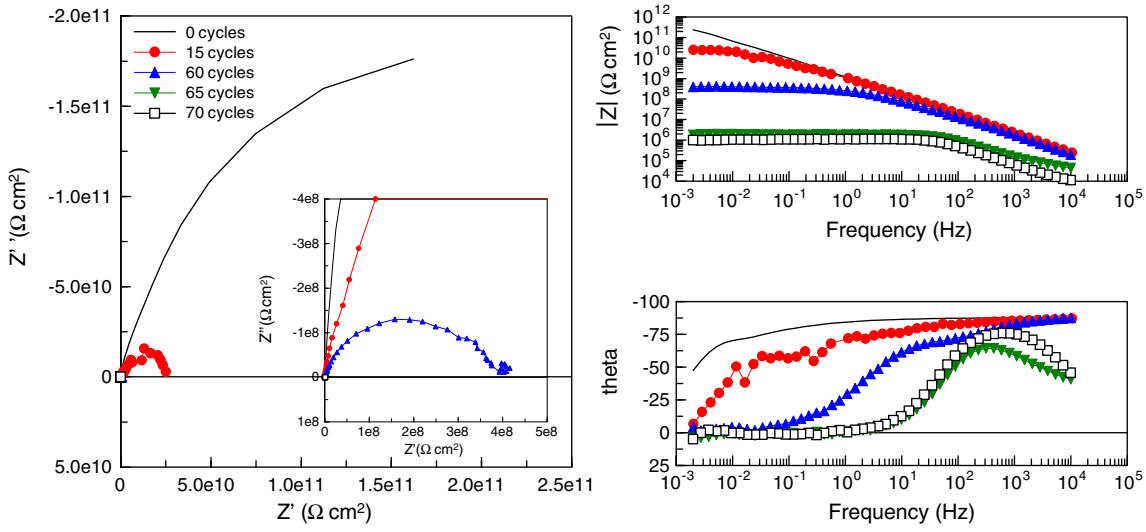

Fig. 13. Nyquist and Bode plots of PEO + polymer specimen (ac/dc/ac procedure).

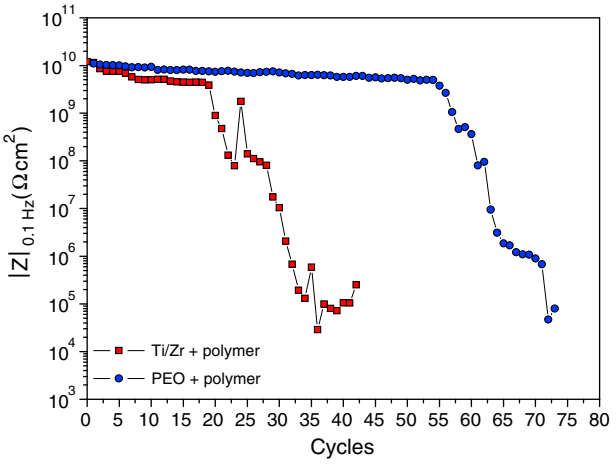

Fig. 14. Low-frequency impedance modulus of Ti/Zr + polymer and PEO + polymer specimens as a function of number of ac/dc/ac cycles.

initiation of localized corrosion) and CPE_2R_2 (capacitive behavior and resistance of the inner, barrier part of the coating, including that of the coating/substrate interface) (Fig. 8b).

Table 4 shows the values obtained by fitting the equivalent circuits of Fig. 8 to the impedance data in Figs. 6 and 7 (chi-squared values fell within 0.001–0.0001 range). The OCP values of the AZ31 alloy were in the range of −1.517/−1.546 $V_{Ag/AgCl}$. PEO treatment of the magnesium substrate resulted in increased OCP values by up to ~100 mV, which is typical of PEO coatings on magnesium alloys [24]. In case of the AZ31 alloy, R_{ct} values were similar to those obtained in previous studies [46] and CPE_{dl} values were typical of a corroding metal in an electrolyte solution [47].

For the PEO coated specimen, small R_1 values indicated a relatively open access of the electrolyte into the outer coating region. This is in agreement with the electron-optic examination of the coating, which revealed interconnected defects (pores and cracks) in its outer region. The initial high R_2 value, of the order of $2\times10^6\ \Omega\ cm^2$, indicated a dominating contribution of the barrier layer to the corrosion protection of the magnesium substrate [48,49]. However, with increasing immersion time, the significant decrease of R_2 indicated degradation of the barrier layer and initiation of the electrochemical reaction between the magnesium substrate and the electrolyte. The initial value of the CPE_2 corresponds to approximately 120 nm of compact oxide material, according to the well-known relationship:

$$d = \frac{\varepsilon_0 \varepsilon A}{C} \tag{2}$$

where d is the capacitor thickness (m), ε_0 is vacuum permittivity (8.85 F m^{-1}), ε is relative permittivity of pure MgO (~9.8 F m^{-1}), C is capacitance (F) and A is surface area (m^2).

Increasing CPE_2 values corroborate increasing number of defects in the barrier layer. The deterioration of the barrier layer was possibly caused by the volume expansion and stresses generated during hydration of MgO into $Mg(OH)_2$ [45,50].

Figs. 9 and 10 show the impedance spectra of polymer coated specimens after immersion in 5 wt.% NaCl solution for different times up to 77 days. Initially, both Ti/Zr + polymer and PEO + polymer coatings showed impedance values of the order of $10^{10}\ \Omega\ cm^2$ in the low-frequency region, which are higher than other values reported in the literature for polymer coated magnesium alloys [4,14,19,45,51,52]. As shown in Fig. 11, the total impedance of polymer-coated specimens slightly decreased with the exposure time, suggesting the diffusion of water and other ions through the coating [4]. Nevertheless, after 77 days of exposure, the impedance modulus at 0.1 Hz remained high (~$10^9\ \Omega\ cm^2$) for both Ti/Zr + polymer and PEO + polymer coatings. This indicated an adequate corrosion protection of the surface.

For the initial 7 days of immersion, the equivalent circuit in Fig. 8c was used for interpretation of the EIS data of polymer-coated specimens. This circuit comprises R_e (electrolyte resistance), CPE_1R_1 (capacitive behavior and resistance of the polymer coating) and a finite length Warburg component, associated with the diffusion of charged electrolyte species across the polymer film. The Warburg impedance (short circuit terminus model) is described by the formula:

$$Z_W = \frac{R\tanh\left([jT\omega]^P\right)}{(jT\omega)^P} \tag{3}$$

where R is the so-called limiting diffusion resistance, T is a time constant, related to the diffusion process coefficient (D_{dif}) and length (L): $T = L^2/D_{dif}$, and P is an exponent to describe the capacitive character of

Table 6
Data of the equivalent circuits of polymer-coated specimens (ac/dc/ac procedure).

	0 cycles	7 cycles	15 cycles	30 cycles	40 cycles
Ti/Zr + polymer					
OCP ($V_{Ag/AgCl}$)	−1.239	−1.220	−1.226	−1.292	−1.519
CPE_1-*T* ($S\ s^P/cm^2$)	6.70×10^{-11}	6.80×10^{-11}	6.98×10^{-11}	3.53×10^{-10}	1.75×10^{-8}
CPE_1-*P*	0.98	1.00	1.00	0.88	0.93
R_1 ($\Omega\ cm^2$)	2.15×10^8	4.42×10^6	5.23×10^6	2.52×10^5	3.00×10^5
CPE_2-*T* ($S\ s^P/cm^2$)	–	9.31×10^{-11}	6.64×10^{-11}	5.19×10^{-10}	8.89×10^{-5}
CPE_2-*P*	–	0.73	0.79	0.94	0.91
R_2 ($\Omega\ cm^2$)	–	4.12×10^9	1.10×10^7	9.96×10^6	320
W-*R* ($\Omega\ cm^2$)	3.57×10^{11}	6.69×10^{10}	3.59×10^{10}	–	–
W-*T* (s)	104.1	82.4	49.5	–	–
W-*P*	0.61	0.41	0.43	–	–
PEO + polymer					
OCP ($V_{Ag/AgCl}$)	−1.227	−1.234	−1.215	−1.475	−1.529
CPE_1-*T* ($S\ s^P/cm^2$)	6.21×10^{-11}	8.08×10^{-11}	1.00×10^{-10}	3.56×10^{-9}	3.07×10^{-9}
CPE_1-*P*	0.97	0.99	0.98	0.86	0.97
R_1 ($\Omega\ cm^2$)	3.59×10^8	2.6×10^6	1.26×10^6	1.59×10^6	1.03×10^6
CPE_2-*T* ($S\ s^P/cm^2$)	–	1.26×10^{-10}	4.66×10^{-10}	3.86×10^{-9}	1.61×10^{-7}
CPE_2-*P*	–	0.71	0.67	0.90	0.99
R_2 ($\Omega\ cm^2$)	–	4.70×10^9	3.77×10^8	2.50×10^5	6.50×10^4
W-*R* ($\Omega\ cm^2$)	3.73×10^{11}	3.18×10^{10}	–	–	–
W-*T* (s)	110.0	30.2	–	–	–
W-*P*	0.51	0.50	–	–	–

the diffusion. The equivalent circuit in Fig. 8d was used to simulate the impedance behavior after 7 days of immersion, where the CPE_2R_2 element represents the capacitive behavior and resistance of the inner part of the coating system, including that of the Ti/Zr conversion pre-treatment or PEO coating. The presence of the Warburg element in series with R_2 refers to the limited mass transport across the Ti/Zr conversion and PEO coatings.

The circuit elements calculated from the fitting results of the polymer coated specimens are summarized in Table 5. Both Ti/Zr + polymer and PEO + polymer coatings revealed very similar CPE_1 and R_1 values, indicating that the characteristics of the polymer top layer were nearly the same, regardless of the applied pre-treatment. However, R_2 and *W-R* 1parameters, which are associated with the inner region of the coating system, were about an order of magnitude higher for the PEO pre-treatment, indicating higher corrosion resistance of the latter compared with the Ti/Zr pre-treatment. Further, *W-T* parameter, characterizing the life-time of diffusing charged species, was about five times higher for the PEO pre-treatment, which, in conjunction with higher *W-R* values, confirms that better performance of the PEO + polymer coating is associated with the greater role of mass-transfer limitations in inhibition of the corrosion process.

3.3.2. ac/dc/ac results

Given that the polymer coating with both pre-treatments did not fail during EIS measurements after relatively long immersion times and that attempts to predict its failure, based on the evolution of parameters such as polymer capacitance/resistance or low-frequency impedance, were unsuccessful, ac/dc/ac measurements were carried out.

Figs. 12 and 13 show the impedance spectra obtained by applying the ac/dc/ac procedure to the polymer-coated specimens. During the initial cycles, Nyquist and Bode plots resembled those obtained by conventional EIS. Then, as shown in Fig. 14, there was a considerable decrease of the low-frequency impedance modulus after 20 and 55 cycles for the Ti/Zr + polymer and PEO + polymer coatings, respectively. If 10^7 Ω cm^2 is set as a critical value, as suggested by Gray and Appleman [53], then the loss of protective properties occurred after 30 (5 days) and 63 (10 days) cycles for the Ti/Zr + polymer and PEO + polymer coatings, respectively. Therefore, compared with conventional EIS measurements, a much shorter time is needed for the ac/dc/ac method to detect changes in the protective properties of the studied systems.

The equivalent circuits in Fig. 8c–d and b were used to simulate the ac/dc/ac results before and after coating failure, respectively. The calculated values are presented in Table 6 (chi-squared values fell within 0.001–0.0001 range). At the initial stages of the ac/dc/ac test, the protective properties of the Ti/Zr + polymer coating remained intact and the calculated parameters were very similar to those obtained by conventional EIS. However, due to the more stressing conditions used in this test, coating failure occurred after a relatively short period of time. This was manifested by considerable drop in the OCP value and drastic decrease in R_2 value and increase in CPE_2 value, the new values corresponding to the values of charge transfer resistance and double electric layer at the magnesium substrate/electrolyte interface (Table 6). The local damage of the paint layer is evident from the increase of the capacitance CPE_1 by three orders of magnitude, compared with the CPE_1 of undamaged paint. This new CPE_1 value, as well as the two-fold reduced R_1 value, represents the layer of corrosion products in the breach-point, rather than the paint. The same conclusions may be drawn for the PEO + polymer coating, except that the time of failure was delayed by approximately 3 times due to the better anti-corrosion properties of the PEO coating compared with the Ti/Zr conversion treatment. Further, the past-failure value of R_2 is still considerably high, and CPE_2 value corresponds to that of an oxide layer rather than a substrate/electrolyte interface, suggesting that PEO pre-treatment still retains some protective properties.

3.3.3. Atmospheric corrosion tests

Surface appearance of specimens before and after ASTM B117 and VDA tests is presented in Fig. 15. After exposure for 7 days, corrosion products, mainly consisting of $Mg(OH)_2$ [9], were clearly visible on the surface of untreated AZ31 specimens (Fig. 15a). For both tests, cross-sections revealed pitting corrosion as the dominant mechanism of corrosion, although corrosion penetration depth was higher in the specimen subjected to salt fog test (~1.5 mm) compared with the VDA test (~0.08 mm) (Fig. 16). This is mainly associated with the continuous presence of water and Cl^- ions in the ASTM B117 as opposed to the VDA test, where the drying cycles facilitate the formation of more compact and protective corrosion products.

The PEO-treated AZ31 specimen revealed improved corrosion resistance compared with the bare alloy (Fig. 15b). However, due to the small thickness of the barrier layer and the presence of interconnected pores in the PEO coating, aggressive species reached the substrate and corrosion damage in the form of pitting corrosion was observed after 7 days of exposure. Average pit depths were ~0.8 mm and ~0.1 mm for the ASTM B117 and VDA tests, respectively, whereas pit density was in the range of 0.8–1.0 pits/cm^2 for both tests.

Specimens with the Ti/Zr + polymer and PEO + polymer coatings passed 7 days test duration without showing any signs of surface degradation (Fig. 15c and d). Scribed specimens revealed more significant differences between these coatings, more so after the VDA test (Fig. 15e and f). Thus, according to ASTM D1654 (procedure A) standard, the rating numbers were 5 and 7 for the Ti/Zr + polymer coating and 6 and 10 for the PEO + polymer coating after ASTM B177 and VDA tests for

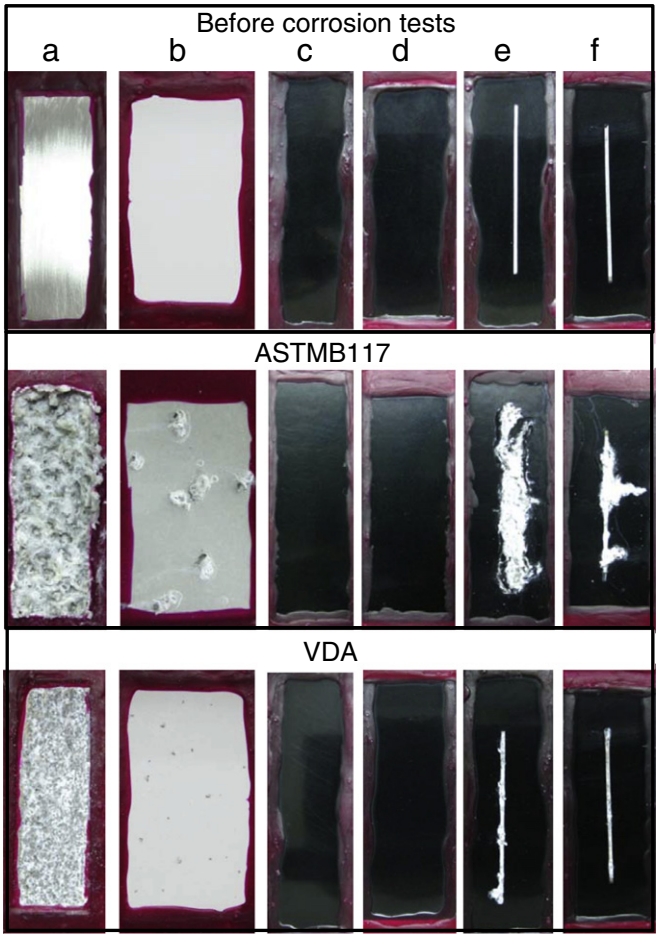

Fig. 15. Surface appearance of studied AZ31 specimens before and after accelerated corrosion tests: (a) untreated, (b) PEO, (c) Ti/Zr + polymer, (d) PEO + polymer, (e) scribed Ti/Zr + polymer and (f) scribed PEO + polymer.

7 days, respectively. Cross-sections of the scribed areas clearly revealed a significant improvement of corrosion resistance of the specimens with PEO coating used as paint pre-treatment. Maximum corrosion penetration depth went down from ~1.5 and ~0.2 mm for the Ti/Zr + polymer specimen to ~0.07 and ~0.04 mm for the AZ31 alloy with the PEO + polymer coating after ASTM B117 and VDA tests, respectively (Fig. 16). This improvement was attributed to the barrier effect of the PEO coating, which delays the interaction between the substrate and the aggressive environment. From these results, it is evident that scribing the panels prior to the atmospheric tests facilitates assessment of the damage level of the coating/substrate system. However, this method is rather subjective, as it is based on visual observation, and it does not provide quantitative information on the barrier properties of the system.

4. Conclusions

1. Mechanical tests revealed an excellent performance of the polymer coating when the Ti/Zr conversion coating was used as a pre-treatment. The PEO + polymer coating showed excellent adhesion and acceptable impact resistance, the latter being inferior to that of the Ti/Zr + polymer coating. This was attributed to higher stiffness of the PEO coating compared with the substrate and polymer layer.
2. EIS measurements showed poor localized corrosion resistance of the uncoated AZ31 magnesium alloy in 5 wt.% NaCl solution, as indicated by the relatively low $|Z|_{0.1Hz}$ values (10^2–$10^3\ \Omega\,cm^2$) and the presence of an inductive loop at low frequencies. PEO treatment significantly increased the corrosion resistance of the AZ31

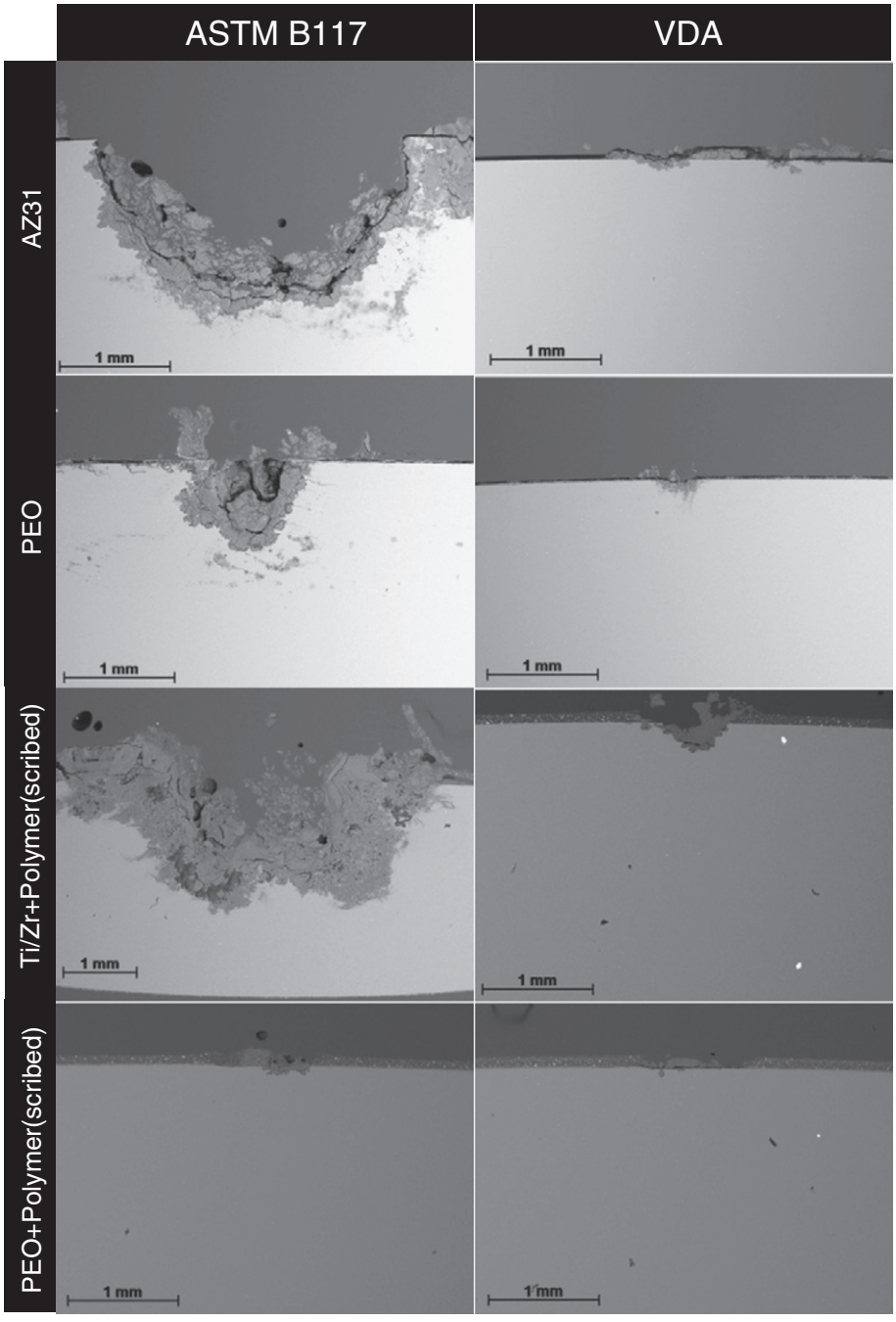

Fig. 16. BSE cross-sections of AZ31 specimens after exposure to ASTM B117 and VDA tests.

alloy ($|Z|_{0.1Hz} = 10^6\ \Omega cm^2$), but only for short immersion times due to the porous nature of the outer region of the PEO coating and deterioration of the inner barrier layer, possibly associated with the volume expansion and stresses generated during hydration of MgO into $Mg(OH)_2$. As for the polymer-coated specimens, high impedance values ($|Z|_{0.1Hz} = 10^9\ \Omega cm^2$) indicated almost negligible degradation of the polymer top-layer after 77 days in 5 wt.% NaCl solution and superior corrosion resistance properties of the PEO pretreatment compared with the Ti/Zr conversion coating. The degradation of the polymer-coated specimens in the ac/dc/ac test was manifested as a sudden decrease in the low-frequency impedance modulus after 30 and 63 cycles for the Ti/Zr and PEO pretreatments, respectively. The degradation mechanism was associated with the loss of the protective properties of applied pretreatments. The ac/dc/ac test gave the same ranking of corrosion resistance as those based on EIS measurements and atmospheric tests with scribed panels.

3. Untreated AZ31 magnesium alloy revealed pitting corrosion after continuous exposure to salt fog per ASTM B117 and cyclic exposure per VDA. PEO treatment of AZ31 resulted in increased corrosion resistance. However, coating failure in the form of pitting corrosion was observed after long term exposure to accelerated corrosion tests. The application of a polymer coating improved the corrosion resistance of the AZ31 alloy. The duplex PEO + polymer coating provided a much more noticeable protection than Ti/Zr + polymer coating as deduced from smaller paint creepage and lower corrosion penetration depth in scribed panels. Compared with the continuous test, the cyclic corrosion test provided more significant differences between tested specimens.

Acknowledgments

The authors are grateful to the MCYT (Spain, Project MAT 2009-09845-C02-01) for the financial support. The authors also acknowledge DECOTEC S.L. (Spain) for the mechanical testing of specimens. R. Arrabal and E. Matykina are grateful to the MICINN (Spain) for the financial support via the Ramon y Cajal Programme (RYC-2008-02038, RYC-2010-06749).

References

[1] E.A. Nyberg, A.A. Luo, K. Sadayappan, W. Shi, Adv. Mater. Processes 166 (2008) 35.
[2] M. Mosialek, G. Mordarski, P. Nowak, W. Simka, G. Nawrat, M. Hanke, R.P. Socha, J. Michalska, Surf. Coat. Technol. 206 (2011) 51.
[3] L.O. Snizhko, A. Yerokhin, N.L. Gurevina, D.O. Misnyankin, A.V. Ciba, A. Matthews, Surf. Coat. Technol. 205 (2010) 1527.
[4] T.F. Conceicao, N. Scharnagl, C. Blawert, W. Dietzel, K.U. Kainer, Corros. Sci. 52 (2010) 2066.
[5] H. Hoche, J. Schmidt, S. Grob, T. Trobmann, C. Berger, Surf. Coat. Technol. 205 (Supplement 2) (2011) S145.
[6] J. Jin, C. Liu, S. Fu, Y. Gao, X. Shu, Surf. Coat. Technol. 206 (2011) 348.
[7] A.L. Yerokhin, X. Nie, A. Leyland, A. Matthews, S.J. Dowey, Surf. Coat. Technol. 122 (1999) 73.
[8] R. Arrabal, E. Matykina, T. Hashimoto, P. Skeldon, G.E. Thompson, Surf. Coat. Technol. 203 (2009) 2207.
[9] R. Arrabal, A. Pardo, M.C. Merino, M. Mohedano, P. Casajús, S. Merino, Surf. Coat. Technol. 204 (2010) 2767.
[10] J.E. Gray, B. Luan, J. Alloys Compd. 336 (2002).
[11] C.E. Tomlinson, Conversion Coatings for Metals Using Group IV-Z Metals in the Presence of Little or No Fluoride and Little or No Chromium, US5952049, 1999.
[12] J.I. Skar, M. Walter, D. Albright, Proceedings of Society of Automotive Engineers, 1997, p. 7.
[13] G. Guerci, C. Mus, K. Stewart, International Congress Magnesium Alloys and Their Applications, 2000.
[14] G.-L. Song, Surf. Coat. Technol. 203 (2009) 3618.
[15] S. Hutchins, P. Shashkov, V. Samsonov, A. Shatrov, Magnesium, Wiley-VCH Verlag GmbH & Co. KGaA, 2005, p. 553.
[16] V. Tchervyakov, G. Gao, J. Bomback, A.P. Pchelnikov, G. Cole, in: H.I. Kaplan, J. Hryn, B. Clow (Eds.), Magnesium Technology 2000, TMS, Nashville, Tennessee, 2000, p. 143.
[17] J.H. Hawkins, 50th Annual World Magnesium Conference, Washington, D.C, 1993.
[18] H. Umehara, M. Takaya, T. Itoh, Magnesium Alloys and their Applications, Wiley-VCH Verlag GmbH & Co., 2006, p. 506.
[19] P.B. Srinivasan, N. Scharnagl, C. Blawert, W. Dietzel, Surf. Eng. 26 (2010) 354.
[20] Y. Jiang, Y. Bao, K. Yang, Magnesium Technology 2011, John Wiley & Sons, Inc., 2011, p. 543.
[21] C. Blawert, W. Dietzel, E. Ghali, G. Song, Adv. Eng. Mater. 8 (2006) 511.
[22] F. Liu, D. Shan, Y. Song, E.-H. Han, Surf. Coat. Technol. 206 (2011) 455.
[23] S. Shrestha, Surf. Eng. 26 (2010) 313.
[24] R. Arrabal, E. Matykina, F. Viejo, P. Skeldon, G.E. Thompson, Corros. Sci. 50 (2008) 1744.
[25] U. Malayoglu, K.C. Tekin, S. Shrestha, Surf. Coat. Technol. 205 (2010) 1793.
[26] S.-J. Kim, J.-I. Kim, M. Okido, Mater. Sci. Forum 486–487 (2005) 129.
[27] S. Hutchins, S. Shrestha, A. Sturgeon, P. Shashkov, A. Shatrov, in: K.U. Kainer (Ed.), Magnesium, Proceedings of the 6th International Conference Magnesium Alloy and Their Applications, 2004, p. 617.
[28] A. Mandelli, M. Bestetti, A. Da Forno, N. Lecis, S.P. Trasatti, M. Trueba, Surf. Coat. Technol. 205 (2011) 4459.
[29] X. Lu, Y. Zuo, X. Zhao, Y. Tang, X. Feng, Corros. Sci. 53 (2011) 153.
[30] Y.F. Jiang, H.S. Yang, Y.F. Bao, Y.Y. Liu, Zhongguo Youse Jinshu Xuebao/Chin. J. Nonferrous Met. 21 (2011) 1562.
[31] M. Bestetti, P.L. Cavallotti, A. Da Forno, S. Pozzi, Trans. Inst. Met. Finish. 85 (2007) 316.
[32] J. Hollaender, E. Ludwig, S. Hillerbrand, Fifth International Tinplate Conference, London, 1992, p. 300.
[33] S. Song, G.-L. Song, W. Shen, DoD Corrosion Conference 2011, La Quinta, CA, 2011.
[34] S. Song, R.C. McCune, W. Shen, Y.-M. Wang, in: W.H. Sillekens, N.R. Neelameggham, S.N. Mathaudhu (Eds.), Magnesium Technology 2011, Wiley, San Diego, California, USA, 2011, p. 531.
[35] J. Suay, M. Rodríguez, R. Izquierdo, A. Kudama, J. Saura, J. Coat. Technol. 75 (2003) 103.
[36] EN ISO 2409, Paints and Varnishes — Cross-Cut Test, CEN, Brussels, Belgium, 2007.
[37] EN ISO 6272-1, Paints and Varnishes — Rapid-Deformation (impact resistance) Tests — Part 1: Falling-Weight Test, Large-Area Indenter, CEN, Brussels, Belgium, 2002.
[38] ASTM B117, Standard Practice for Operating Salt (Fog) Spray Apparatus, Philadelphia, USA, , 2003.
[39] VDA 621-415, Testing of Corrosion Protection of Vehicle Paint by Alternating Cycles Test, Frankfurt, Germany, 1982.
[40] DIN 50014, Climates and Their Technical Application; Standard Atmospheres, Berlin, Germany, 1985.
[41] ASTM D1654, Standard Test Method for Evaluation of Painted or Coated Specimens Subjected to Corrosive Environments, Philadelphia, USA, 2008.
[42] O. Lunder, C. Simensen, Y. Yu, K. Nisancioglu, Surf. Coat. Technol. 184 (2004) 278.
[43] A.L. Yerokhin, A. Shatrov, V. Samsonov, P. Shashkov, A. Leyland, A. Matthews, Surf. Coat. Technol. 182 (2004) 78.
[44] G. Song, A. Atrens, D.S. John, X. Wu, J. Nairn, Corros. Sci. 39 (1997) 1981.
[45] J. Liang, P.B. Srinivasan, C. Blawert, W. Dietzel, Electrochim. Acta 55 (2010) 6802.
[46] A. Pardo, M.C. Merino, A.E. Coy, F. Viejo, R. Arrabal, S. Feliú Jr., Electrochim. Acta 53 (2008) 7890.
[47] A.J. Bard, L.R. Faulkner, Electrochemical Methods; Fundamentals and Applications, 2000.
[48] D.Y. Hwang, Y.M. Kim, D.H. Shin, Mater. Trans. 50 (2009) 671.
[49] S.J. Xia, R. Yue, J.R.G. Rateick, V.I. Birss, J. Electrochem. Soc. 151 (2004) B179.
[50] W. Zhang, B. Tian, K. Du, H. Zhang, F. Wang, Int. J. Electrochem. Sci. 6 (2011) 5228.
[51] S. Sathiyanarayanan, S.S. Azim, G. Venkatachari, Appl. Surf. Sci. 253 (2006) 2113.
[52] M.B. Kannan, D. Gomes, W. Dietzel, V. Abetz, Surf. Coat. Technol. 202 (2008) 4598.
[53] L. Gray, B. Appleman, J. Prot. Coat. Linings (February 2003) 66.